Electronic Supplementary Material (ESI) for Journal of Materials Chemistry C.

Triple $Co^{II, III, IV}$ charge ordering and spin states in modular cobaltites: A systematization through experimental and virtual compounds

R. David[a], H. Kabbour[a*], P. Bordet[b,c], D. Pelloquin[d], O. Leynaud[b,c], M. Trentesaux[a] and O. Mentré[a]

[a] Unité de Catalyse et de Chimie du Solide, Université Lille Nord de France, Villeneuve d'Ascq, France

[b] Univ. Grenoble Alpes, Institut Néel, Grenoble, France

[c] CNRS, Institut Néel, Grenoble, France

[d] CRISMAT, Caen, France

SUPPLEMENTARY INFORMATION

S1: Structures of several compounds within the homologous series with formulae $[BaCoO_3]_n[BaCo_8O_{11}]$: (a) n=1 $Ba_2Co_9O_{14}$, (b) n=2 $Ba_3Co_{10}O_{17}$, and (c) n=5 $Ba_6(Co,Ga)_{13}O_{26}$. (d) Structure of $Ba_2Co_4XO_7$ (*X*= halogen) which exhibits the same $BaCo_8O_8$ building block (Figure below).

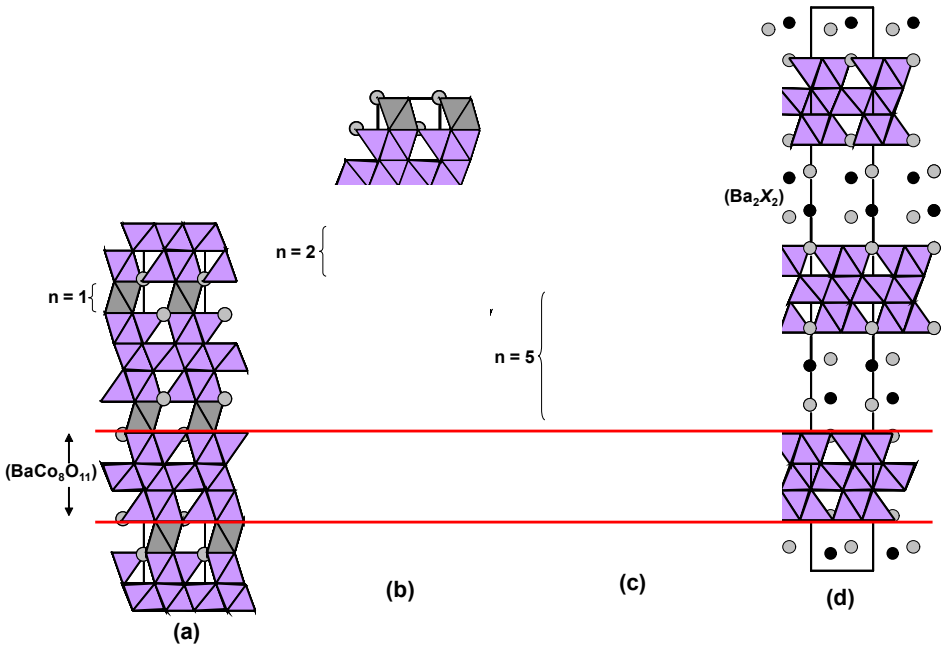

S2: Geometry optimization of the experimental n= 2 term ($Ba_3Co_{10}O_{17}$)

The full relaxations (atomic positions and cell parameters) using GGA only (S1a,c) lead to a good agreement with the experimental structures. The same relaxation using spin-polarized calculations with a ferromagnetic unit cell (S1b) in the case of n= 2 leads to slightly smaller error percentages. A careful analysis of the distances show a good agreement between experience and optimization, all percentages of errors being lower than 5% in the case of non-spin-polarized calculations. Although the spin polarization slightly improve the errors, the non-spin-polarized calculations are sufficiently reasonable. Therefore, we have chosen to work without spin-polarization in order to avoid simplification on the magnetic configuration choice as it may affect the structure, especially for the hypothetical structures for which there is no comparison with experience.

Table S2a. Atomic positions after full relaxation of the experimental structure of $Ba_3Co_{10}O_{17}$. The relaxed unit cell parameters are: a= 5.683 Å and c= 35.822 Å (Space group $R\bar{3}m$). The deviations from experience are ≤ 0.4% for both unit cell parameters and ≤ 1.5% for all atomic positions.

Atom	Wyck.	x	y	z
Ba1	3a	0	0	0
Ba2	6c	2/3	1/3	0.9329
Co1	3b	1/3	2/3	1/6
Co2	9d	5/6	1/6	1/6
Co3	6c	0	0	0.3065
Co4	6c	0	0	0.2322
Co5	6c	2/3	1/3	0.2475
O1	18h	0.6816	0.8408	0.1951
O2	6c	0	0	0.1385
O3	18h	0.4888	0.5112	0.4027
O4	9e	1/2	1/2	0

Table S2b. Atomic positions after full relaxation of the experimental structure of $Ba_3Co_{10}O_{17}$ using spin-polarized (FM) calculations. The relaxed unit cell parameters are: a= 5.7217 Å and c= 35.8680 Å (Space group $R\bar{3}m$). The deviations for both unit cell parameters and atomic positions compared to experience are all ≤ 0.5%.

Atom	Wyck.	x	y	z
Ba1	3a	0	0	0
Ba2	6c	2/3	1/3	0.9330

Co1	3b	1/3	2/3	1/6
Co2	9d	5/6	1/6	1/6
Co3	6c	0	0	0.3056
Co4	6c	0	0	0.2325
Co5	6c	2/3	1/3	0.2471
O1	18h	0.6932	0.8466	0.1965
O2	6c	0	0	0.1392
O3	18h	0.4878	0.5122	0.4022
O4	9e	1/2	1/2	0

S3. Optimized structures in terms n=2 and n=3 for both cubic and hexagonal packing using the calculations conditions chosen in S1 (simple GGA non spin-polarized).

Table S3a. Structural parameters of the optimized *n*=2 terms: cubic and hexagonal packing

Unit cell parameters and space group	Atom type	Wyckoff position	x	y	z
Cubic packing					
a= 5,690 Å c= 35,937 Å $R\bar{3}m$	Ba1	*-3m*	0	0	0
	Ba2	*3m*	0,666667	0,333333	0,93188
	Co1	2/m	0,833333	0,166667	0,166667
	Co2	*3m*	0	0	0,30605
	Co3	*3m*	0	0	0,23147
	Co4	*-3m*	0,333333	0,666667	0,166667
	Co5	*3m*	0,666667	0,333333	0,24519
	O1	m	0,692	0,846	0,19704
	O2	*3m*	0	0	0,14
	O3	m	0,4877	0,5123	0,4023
	O4	2/m	0,5	0,5	0
Hexagonal packing					
a= 5,6848Å c= 24,1882 Å $P\bar{3}m1$	Ba1	*3m*	0	0	0,153608
	Ba2	*3m*	0	0	0,345192
	Ba3	*3m*	0,333333	0,666667	0,249889
	Co1	*3m*	0,666667	0,333333	0,300232
	Co2	*3m*	0,666667	0,333333	0,199459
	Co3	*3m*	0,333333	0,666667	0,379409
	Co4	*3m*	0,666667	0,333333	0,095662
	Co5	*-3m*	0	0	0
	Co6	*-3m*	0	0	0,5
	Co7	2/m	0,5	0	0
	Co8	2/m	0,5	0	0,5
	Co9	*3m*	0,333333	0,666667	0,120708
	Co10	*3m*	0,666667	0,333333	0,404125
	O1	*3m*	0,333333	0,666667	0,041798
	O2	*3m*	0,333333	0,666667	0,458129
	O3	m	0,512809	0,025619	0,144037
	O4	m	0,512585	0,025169	0,355814
	O5	m	0,826469	0,173531	0,457999
	O6	m	0,347469	0,173735	0,041886

	O7	m	0,816796	0,183204	0,249844

Table S3b. Structural parameters of the optimized *n*=3 terms: cubic and hexagonal packing

Unit cell parameters and space group	Atom type	Wyckoff position	x	y	z
Cubic packing					
a= 5.665370Å c= 14.283940Å $P\bar{3}$m1	Ba1	3m	0.000000	0.000000	0.256980
	Ba2	3m	0.333333	0.666667	0.426720
	Co1	3m	0.333333	0.666667	0.645930
	Co2	-3m	0.000000	0.000000	0.500000
	Co3	3m	0.333333	0.666667	0.835720
	Co4	-3m	0.000000	0.000000	0.000000
	Co5	2/m	0.500000	0.000000	0.000000
	Co6	3m	0.333333	0.666667	0.203720
	O1	3m	0.333333	0.666667	0.071400
	O2	m	0.511320	0.022650	0.242480
	O3	m	0.174060	0.825940	0.928720
	O4	m	0.835380	0.164620	0.415040
Hexagonal packing					
a=5.6953 Å c= 43.3004 Å $R\bar{3}m$	Ba1	6c	2/3	1/3	0.24588
	Ba2	6c	2/3	1/3	0.14600
	Co1	3a	0	0	0
	Co2	9e	1/2	1/2	0
	Co3	6c	1/3	2/3	0.22310
	Co4	6c	1/3	2/3	0.28048
	Co5	6c	0	0	0.26519
	Co6	3b	1/3	2/3	1/6
	O1	18h	0.63997	0.81998	0.25366
	O2	6c	2/3	1/3	0.02365
	O3	18h	0.65253	0.82626	0.02316
	O4	18h	0.18398	0.81602	0.13789

S4. Comparison of the density of states (DOS) projected on the *d* states of Co atoms for different terms and stacking type (*h* or *c*).

Figure S4 below: Topologies of the Density of States (DOS) projected on the cobalt *d* states for each type of cobalt atom sites for rows (a) the *n*= 1 experimental term $Ba_2Co_9O_{14}$, (b) the *n*= 2*c* (cubic) experimental phase (C-$Ba_3Co_{10}O_{17}$), (c) the *n*= 2*h* (hexagonal) hypothetical phase (H-$Ba_3Co_{10}O_{17}$), (d) for the *n*= 3*c* hypothetical term C-$Ba_4Co_{11}O_{20}$ and (e) for the n= 3*h* hypothetical term H-$Ba_4Co_{11}O_{20}$. The DOS were calculated for a simple ferromagnetic unit cell in the GGA approximation. DFT+U calculations were not employed to avoid any artificial stabilization of high spin states.

The Fermi level is indicated by vertical dotted lines. Spins *up* and *down* are represented as ↑and↓, respectively.

The plots are annotated with the corresponding Co atom as follows:

- For the [$BaCo_6O_9$] block (first three columns): Co(Td) corresponds to the tetrahedral sites. Co(Oh CoO_2) corresponds to the magnetic atomic sites within the CdI_2 type layer (edge sharing octahedrons layer). Co(Oh CoO_2 non mag) corresponds to the non-magnetic atomic sites within the same CdI_2 type layer.
- For the [$Ba_nCo_{2+n}O_{3n+2}$] block (three last columns): Co(Oh central) corresponds to the central Oh in the perovskite layer. Co(Oh edge) corresponds to the octahedral site within the layer of polyhedrons involving tetrahedrons and the Co(Oh edge) sandwiched between the CdI_2 type layer and the other octahedrons of the perovskite layer. Co(Oh intermed.) is used to account for the additional site in the perovskite block for the *n*= 3 terms, located between the Co(Oh central) and the Co(Oh edge).

The disposition into columns of analogous sites allows a direct comparison. The spin states (HS/LS) are indicated in red for the sites holding variations within the series.

S5. XPS measurements

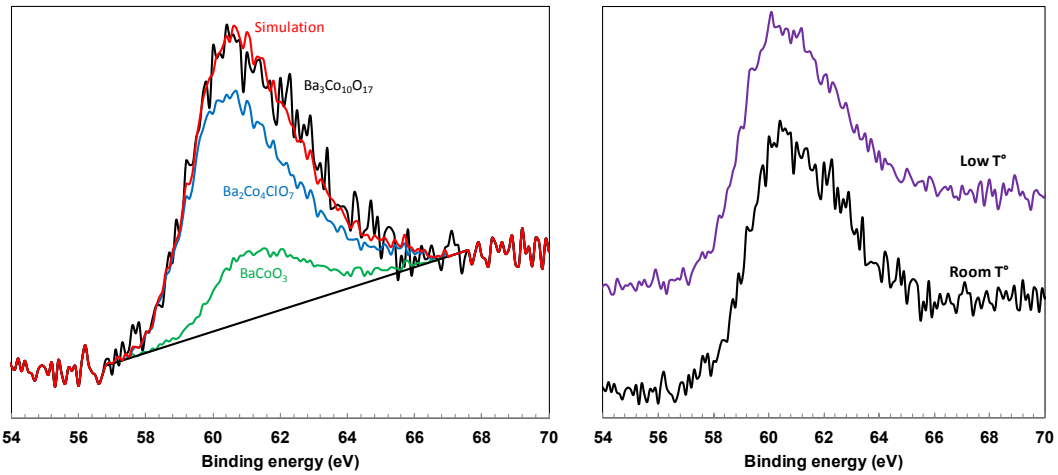

Figure S5. XPS measurements. (left) Spectra of $Ba_3Co_{10}O_{17}$ (black), of the references $BaCoO_3$ (green) and $Ba_2Co_4ClO_7$ (blue), and simulation of $Ba_3Co_{10}O_{17}$ using both references (red). (right) Comparison between the low temperature and room temperature measurements

S6. Additional experimental details of the low temperature single crystal XRD

The sample is glued to a quartz fiber and centered on a two-axis mini-goniometer magnetically coupled to the diffractometer φ axis. The coupling is achieved by mounting a master magnet in place of the usual goniometer head. The mini goniometer is inserted inside an orange-type LHe bath cryostat which is supported independently from the diffractometer and equipped for crystal centering in the x-ray beam, the crystal being observed either optically through mylar windows or by its x-ray absorption and/or diffraction signal. The cryostat can be rotated about the vertical axis by 30° steps. It is equipped with a flat Be exit window allowing to use the full active surface of the detector at a minimum sample-detector distance of 35mm. Here, the normal to the cryostat exit window was rotated at 30° from the direct x-ray beam, and the detector was placed at a fixed θ=15° position.